RSC Advances

ROYAL SOCIETY OF CHEMISTRY

www.rsc.org/advances

Multilayer composite beads constructed via layer-by-layer self-assembly for lysozyme controlled release

Jiemin Zhao [a,b,1], Xiaoping Wang [c,1], Yanshen Kuang [d], Yufeng Zhang [b], Xiaowen Shi [a], Xingyun Liu [a], Hongbing Deng [a,*]

[a] Department of Environmental Science, Hubei Key Lab of Biomass Resource Chemistry and Environmental Biotechnology, School of Resources and Environmental Science, Wuhan University, Wuhan, 430079, China

[b] Hubei-MOST KLOS & KLOBME, Wuhan University Stomatological Hospital, Wuhan University, Wuhan 430079, China

[c] Department of Thoracic Surgery, Tangdu Hospital, Fourth Military Medical University, Xi'an, 710038, China

[d] Zhongnan Hospital, Wuhan University, Wuhan 430079, China

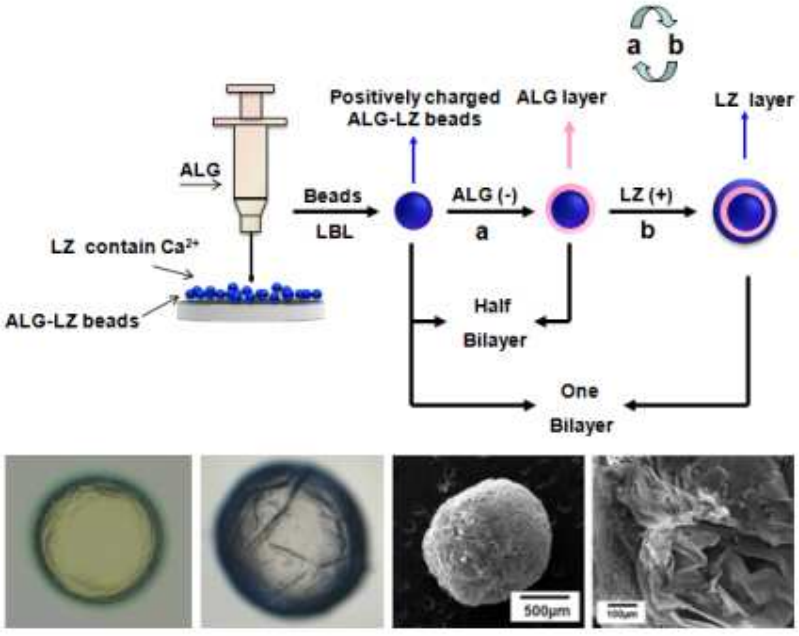

Multilayer composite beads constructed via layer-by-layer self-assembly for lysozyme controlled release

Jiemin Zhao [a,b,1], Xiaoping Wang [c,1], Yanshen Kuang [d], Yufeng Zhang [b], Xiaowen Shi [a], Xingyun Liu [a], Hongbing Deng [a,*]

[a] Department of Environmental Science, Hubei Key Lab of Biomass Resource Chemistry and Environmental Biotechnology, School of Resources and Environmental Science, Wuhan University, Wuhan, 430079, China

[b] Hubei-MOST KLOS & KLOBME, Wuhan University Stomatological Hospital, Wuhan University, Wuhan 430079, China

[c] Department of Thoracic Surgery, Tangdu Hospital, Fourth Military Medical University, Xi'an, 710038, China

[d] Zhongnan Hospital, Wuhan University, Wuhan 430079, China

*Corresponding author. Tel.: +86-2768778501; Fax: +86-2768778501

E-mail address: hbdeng@whu.edu.cn; alphabeita@yahoo.com (H. Deng)

[1] These authors contributed equally to this work.

Abstract

The alginate (ALG)-lysozyme (LZ) beads were fabricated by cross-linking process. Negatively charged ALG and positively charged LZ were alternately deposited on the positively charged ALG-LZ beads via layer-by-layer (LBL) self-assembly technique. The mechanical properties and the enzymatic activity of those samples were studied by regulating the number of deposition bilayers and the composition of the outermost layer. The scanning electron microscopy images indicated that the resultant samples exhibited good sphericity and porosity. The Fourier transform infrared spectra results implied the presence of electrostatic interaction between ALG and LZ. The pore size distribution results revealed that the samples mainly possessed mesopores with radius in the range of 2-7 nm. *In vitro* LZ release test performed at different time intervals showed that LZ could be released from ALG-LZ beads and LBL film-coated beads. Besides, the amount of released LZ increased with extended time intervals.

Keywords: Alginate; Lysozyme; Layer-by-layer self-assembly; control release

1. Introduction

Recently, significant efforts have been made to develop kinds of different protein delivery systems [1-4]. Design of novel protein delivery systems was required for the development of successful product, reduction of adverse reactions and side effects, convenient model of delivery and so on [5]. Herein, various measures have been taken to facilitate the delivery of protein. The application of microspheres and beads was an useful method for protein delivery, which could protect the protein from their microenvironment and keep their long-term biological activity [6, 7].

Based on the above considerations, the carriers for protein delivery should be critically evaluated by considering their toxicity, biological activity and biodegradability *etc*. Additionally, many research efforts were aimed towards choosing alginate (ALG) as an ideal candidate for protein delivery due to its nontoxicity, good biocompatibility and biodegradability *etc*. In detail, it was a family of linear anionic polysaccharide, which consisted of (1-4) linked β-D-mannuronic acid and α -L-guluronic acid units in various composition and sequence and existed widely in many species of brown seaweeds [8, 9]. ALG was studied extensively in drug delivery systems because its droplets could be transformed into rigid beads by gelation with the addition of divalent cations in aqueous solution, such as calcium or barium ions [10]. The relatively mild gelation process enabled proteins to be incorporated into ALG beads with retention of full biological activity, so ALG beads were considered as a perfect carrier for protein delivery.

Owing to the high stability of lysozyme (LZ) within a wide range of pH and

temperature, LZ was chosen as the model protein for drug delivery [11, 12]. LZ, the natural defense substance produced by living organisms with an isoelectric point value of 10.7 [13], was selected as the target protein for its positive charge in aqueous solutions. Moreover, LZ has been extensively used for antibacterial agents [14, 15], wound dressing [16] and protein separation [17]. Compared with the free LZ, immobilized LZ exhibited improved stability to environmental changes. There were many investigations focused on the immobilization of LZ [13, 18, 19]. In our research, the major means of immobilizing LZ was encapsulation, which could fabricate rigid beads by dropping ALG into excessive LZ solutions containing calcium ions. Interestingly, after the encapsulation, the surface of beads was positively charged with LZ on the outmost layer. Although the significance of protein immobilization has been stressed, few researches have paid attention to the further immobilization of protein on the surface of protein loaded template. Here, the technique applied for further immobilization of much more LZ was electrostatic layer-by-layer self-assembly technique (LBL), which has rapidly spread within various researchers due to the simplicity of the procedure [19-21]. Based on this technology, relatively high concentrations of the solute in solution led to excess adsorption of the solute where charge neutralization and resaturation resulted in charge reversal. Alternation of the surface charge resulted in a continuous assembly between negatively and positively charged materials affording great freedom in the number of layers [22-24].

In this paper, ALG-LZ beads were firstly produced via cross-linking process. Encouraged by our recent progress on the deposition of LBL films on electrospun

nanofibers [20, 25], negatively charged ALG and positively charged LZ were alternately deposited on the surface of ALG-LZ beads through LBL self-assembly technique. The effect of the outermost layer variation and the number of coating bilayers on the formation of the LBL films deposited ALG-LZ beads were explored. Additionally, the catalytic activity of immobilized LZ was measured and the *in vitro* release experiments were carried out to determine the feasibility of the immobilized LZ release from ALG-LZ beads and LBL films coated beads.

2. Materials and methods

2.1. Materials

The starting materials included as follows: sodium alginate (ALG, $M_w = 2.5\times10^5$ Da) was from Aladdin Chemical Reagent, China. Lysozyme (LZ, activity 25,000 $U\cdot mg^{-1}$) was purchased from Amresco Co., USA. *Micrococcus Lysodeikticus* used for checking the catalytic activity of LZ was supplied by Nanjing Jiancheng, Bioengineering Institute, China. Coomassie Brilliant Blue (G250) was obtained from Amresco Co., USA. Other chemical reagents used in this experiment were analytical grade.

2.2. Fabrication of Beads

According to the previous report [26], ALG-LZ beads were prepared by using cross-linking process. The schematic diagram of the beads formation was shown in scheme1. Briefly, ALG and LZ solutions were dissolved in purified water, and their concentrations were both fixed at 2%. Then, using a hypodermic syringe the prepared ALG solutions were dropped slowly into excessive LZ solutions containing Ca^{2+} (1%,

w/w). The LZ solutions were still under gentle magnetic stirring at room temperature during the dripping process. The obtained beads were filtered and washed.

2.3. Preparation of dipping solutions for LBL process

The dipping solutions for LBL process including the negatively charged ALG solutions and the positively charged LZ solutions with the same concentration of 1 mg/mL by pouring them into purified water. The pH values of ALG and LZ solutions were adjusted at 4 and 6.5, respectively. The ionic strength of all the dipping solutions was regulated by the addition of sodium chloride with the concentration of 0.1 mol/L.

2.4. Formation of LBL structured composite beads

The fabrication process of the LBL structured beads was identical with that in our previous reports [14, 20]. Briefly, the LBL films coated beads were fabricated by adsorption of negatively charged ALG (-52.0 mV) and positively charged LZ (+25.0 mV) on the surface of positively charged ALG-LZ beads (+37.8 mV). First, ALG-LZ beads were soaked with ALG suspensions for 20 min, and then rinsed in pure water baths for 2 min and repeated three times. The beads were then immersed into the LZ solutions for 20 min followed by identical rinsing procedures. The adsorption and rinsing steps were repeated until the desired number of deposition bilayers obtained. Then the composite beads were filtered and froze dried for further characterizations. Herein, $(ALG/LZ)_n$ was used as a formula to label the LBL structured films, where n was the number of (ALG/LZ) bilayers. When n equaled to 5 or 10, the outermost layer on the composite beads was LZ. When n equaled to 5.5 or 10.5, the outermost layer was ALG.

133 2.5. Characterizations

134 The scanning electron microscopy (SEM, JSM-6700F, JEOL Co., Ltd., Japan) was
135 applied to observe the morphology of the beads. Fourier transform infrared (FT-IR)
136 spectra were recorded by using a Nicolet 170-SX (Thermo Nicolet Ltd. USA). The N_2
137 adsorption isotherm data collected at 77.3 K (Autosorb-1-MP, Quantachrome Co.,
138 USA) was applied for evaluating BET surface areas of the prepared samples. Prior to
139 analysis, adsorbent samples were outgassed for 12 h at 313 K. Pore size distribution
140 analysis was performed by conducting N_2 adsorption experiments, and pore volume
141 was calculated using the BJH method [27]. The mechanical properties of the developed
142 structures were examined by a texture analyzer TA.XT2i TA.XTplus (SMS) at a test
143 speed of 2 mm/s with 90% strain.

144 2.6. Measurement of LZ activity

145 The determination of LZ activity was using the M. *lysodeikticus* Fleming (turbidity)
146 method. The activity measurement of free LZ was identical with our former report [14].
147 The activity of immobilized LZ was evaluated according to the method of free LZ
148 determination. 1 mg freeze-dried beads were added into the cuvette to conduct the
149 test.

150 2.7. *in vitro* LZ release profiles

151 The LZ release experiments were done in 10 mmol/L phosphate buffer with the pH
152 value of 7.3 [28]. 10 mg beads were put into a centrifuge tube containing 10 mL of the
153 above solution, and then incubated on a constant temperature shaking bed with 100
154 rpm at 37 ℃. With 4h or 24 h intervals, 1 mL medium was withdrawn and

immediately replaced with the same amount of fresh medium. The amounts of released LZ were determined using Coomassie Brilliant Blue (G250) method through UV-1800 spectrophotometry at 595 nm. All experiments were done in triplicate and mean values were reported. The above mentioned method, commonly referred as the Bradford assay, was based on the absorption shift from 470 to 595 nm when the brilliant blue G dye binds to protein. The brilliant blue G dye bound most readily to arginyl and lysyl residues in the protein, which could lead to variation in the response of the assay to different proteins. The preparation for the Coomassie Brilliant Blue solution was as follows: a total of 100 mg of Coomassie Brilliant Blue G-250 was dissolved in 50 ml of 95% ethanol solution. 100 ml 85% phosphoric acid (w/v) solution was added and then the blending solution was diluted to 1 L with distilled water.

3. Results and Discussion

3.1. Particle size and mechanical properties of beads

The particle size was measured with a micrometer caliper. The data was shown in Table 1. Obviously, the diameter of the wet beads ranged from 1.5 to 3.0 mm, and that of the freeze dried beads ranged from 1.3 to 2.7 mm. The average diameter of the beads slightly increased with the increasing number of coating films both in wet and dry state. The average thickness of each bilayer of the LBL films coated beads could be estimated to 225 ± 0.0007 (n=5/5.5) and 127 ± 0.0007 (n=10/10.5) nm, respectively.

Fig. 1 shows the mechanical properties including the hardness (Fig. 1A) and the

resilience (Fig. 1B) of the beads. Both the hardness and the resilience of the ALG-LZ beads were higher than those of ULBL film-coated beads, which were attributed to the sufficient soaking time and the increasing amount of LZ. LZ was a kind of alkaline enzyme which had low hardness [29], thus the hardness of the beads with the outermost layer of ALG (Figs. 1A5.5 and 10.5) was a little higher than that with LZ on the outermost layer (Figs. 1A5 and 10).

3.2. Morphology of the beads

Fig. 2 presents the SEM images of ALG-LZ beads and LBL films coated beads after freeze-drying treatment. Coincide with our previous report [30], the SEM images of the beads displayed good sphericity and porosity. In order to investigate the influences of the number of coating bilayers on the formation of LBL films coated beads, different number of LBL structured films were deposited on ALG-LZ beads. With the different number of coating bilayers, the morphology of the LBL structured beads was different from each other. The surface of the LBL films coated beads became coarse which was distinguished from that of the uncoated beads, verifying that the polymers were successfully assembled on the surface of the ALG-LZ beads [31]. Interestingly, the surface roughness of LBL films coated beads was clearly observed. The figures show the cross-section of ALG-LZ beads and $(ALG/LZ)_{10.5}$ films coated beads and high magnification image of the surface of the $(ALG/LZ)_{10.5}$ films coated beads, respectively. Remarkably, the pores were both on the surface and internal section of beads. The reason for the presence of the small pores on the surface of LBL films coated beads was that the LBL films were split into webs during the drying

process [20], the formation of the pores on the internal section was ascribed to the pressure developing inside the beads, and some of that pressure could be released from the pores. When more polymers were coated on the surface of beads, they could contribute to the structural support of beads during the solvent evaporation [32], so more polymers coated resulted in less pores inside beads. Because of the high treacliness of the ALG solution, the beads were produced with a tiny tail-like part (Figs. 2b and d).

The porous structure was assumed to affect drug release ability. The N_2 adsorption and desorption isotherm, the pore size distribution were performed (Fig. 3). The cumulative surface area of ALG-LZ beads and $(ALG/LZ)_{10.5}$ films coating was 28.2 and 13.076 m^2/g, respectively. Obviously, the cumulative surface area of the LBL films coated beads was smaller than that of ALG-LZ beads, which further confirmed that the LBL structured films modification was effective. As mentioned above, the deposition space on the beads was limited and could be filled with the polymers via LBL deposition, so the surface area of the beads would become smaller with increasing the number of coating bilayers. On the basis of BJH results, the beads before and after LBL modification mainly possessed mesopores with radius in the 2-7 nm, and the LBL films coated beads had more mesopores with radius in the 4-7 nm than ALG-LZ beads. After LBL modification, pores with different size could be observed from BJH curves (Figs. 3b' and c'), which presumably related to the freeze-drying treatment. According to the previous report [33], the porosity of ALG gel could be affected by drying the beads and complete dehydration of ALG beads could resulted in surface cracking.

221 3.3. FT-IR analysis

222 The FT-IR spectra of composite beads and raw materials were shown in Fig. 4. In
223 the spectrum of ALG [34], the characteristic peaks at 3430, 1615 and 1417 cm^{-1} stood
224 for the -OH groups vibration, asymmetric and symmetric -COO- stretching vibrations,
225 respectively. The bands around the 1030 cm^{-1} (C-O-C Stretching) and 950 cm^{-1} (C-O
226 Stretching vibration) were ascribed to its saccharine structure. As we know, the amide
227 linkages between amino acid residues in polypeptides and proteins gave the
228 well-known fingerprints in their FT-IR spectra, displaying the character of those
229 substances. In the FT-IR spectra of proteins, the position of the amide I band acted as
230 a sensitive indicator of conformation changes in the protein secondary structure [35],
231 and the position of the amide I peak around 1650 cm^{-1} could be observed in LZ,
232 ALG-LZ beads and LBL films coated beads, which indicated that the secondary
233 structure of the protein was retained in the immobilized LZ molecules. The peak at
234 1450 cm^{-1}, corresponded to the C-C stretching vibration of LZ molecules [36].
235 Additionally, the peak of -COO- became widely at 1417 cm^{-1} and the peak at 1530
236 cm^{-1}, corresponding to the amide □ band even disappeared, which indicated that the
237 carboxyl group of ALG interacted with the amino group of LZ.

238 3.4. Enzymatic catalysis

239 The activity of immobilized LZ was listed in Fig. 5. The results were obtained from
240 the freeze-dried samples and free LZ was employed as control. The enzymatic activity
241 of LZ immobilized on ALG-LZ beads was only 18.78% of that of free LZ. The
242 decrease in activity was likely due to the amount of LZ aggregates formed as the

result of encapsulation procedure [37]. The activity of immobilized LZ on $(ALG/LZ)_n$ films coating was higher than that of ALG-LZ beads. The ratio of the activity of immobilized LZ on $(ALG/LZ)_5$ and $(ALG/LZ)_{5.5}$ films coating and free LZ was 41.14% and 35.73%, respectively. It revealed that when the number of coating films reached 5 or 5.5, catalytic activity of the samples with LZ on the outermost layer was higher than that with ALG on the outermost layer , but when the number of coating films reached 10 or 10.5, the catalytic activity of the samples with ALG on the outermost layer was higher than that with LZ on the outermost layer. The reason for the above results was explained as follows: after the first step of LBL, the beads showed low catalytic activity because ALG was on the outermost layer of ALG-LZ beads. After LZ was assembled on the surface of the beads, the beads were covered with LZ, which could contact with M. *lysodeikticus* directly, resulting in high catalytic activity. However, when the number of coating films reached 10 or 10.5, with the thickness of each bilayer of the LBL films coated beads became thin, the hindered diffusion of LZ caused by ALG got weaken accordingly. Besides, as much more LZ deposited on the surface of film-coated beads, the catalytic activity of the samples with ALG on the outermost layer was higher than that with LZ on the outermost layer.

Herein, ALG and LZ were successfully assembled on the surface of ALG-LZ beads via LBL technique. After immobilization, the catalytic activity of LZ was still maintained, and with the different number of coating films, different parameters dominated the catalytic activity of the samples. According to previous literatures, ALG could interact with various kinds of proteins in a protective or destructive

manner. Obviously, it deduced that ALG had a protective effect on immobilized LZ[38].

3.5. *In vitro* release profiles

In order to explore the controlled release properties of ALG-LZ and LBL films coated beads, *in vitro* release experiments were performed at different time intervals. Fig. 6 shows that LZ could be released from both ALG-LZ beads and LBL films coated beads. Obviously, the initial burst phenomenon was exhibited in all samples which could be attributed to the diffusion of water molecules into the polymeric beads structure, leading to the release of immobilized LZ into aqueous solutions from the beads [39]. Actually, beads made from a high α -L-guluronic acid would reswell only slightly upon rehydration, so all beads immersed in phosphate buffer had similar swelling behavior which caused the previously mentioned diffusion [40]. Besides, the equivalent release rates of immobilized LZ released from the LBL structured beads could be observed. Moreover, in the controlled release test, more LZ could be released from LBL films coated beads than that from uncoated beads, which confirmed that it is effective for the LBL self-assembly technique intended to immobilize more LZ.

Fig. 6a presents that the ALG-LZ beads had lower initial release quantity (2.88%) than that of LBL films coated beads (13.16%) during the period of 8h, which resulted from the insufficient immersion time for the degradation of ALG and few LZ loading on the uncoated beads. Besides, LBL films had the lower densities that could promote materials diffusion[41], and the release of LZ could be related to a difference in the diffusion barrier at the surface of the beads [42].

Obviously, in Fig. 6b, the amount of LZ released from ALG-LZ beads was twice as

much as that from ALG-LZ beads in Fig. 6a, because of the long time immersing in medium containing phosphate ions which caused the degradation of Ca^{2+} crosslinked ALG gel by removal of the Ca^{2+} ions [43]. Besides, the amount of LZ released from all the beads reached maximum after 24 h (Fig. 6b), which was presumably ascribed to the diffusion of immobilized LZ through the pores. It demonstrated that with growing number of coating films, both the porosity of the beads and the degradative phosphate ions in the release medium had the great influences on the LZ release profiles. Fig. 6b presents that more LZ could be released from the $(ALG/LZ)_{10}$ or $(ALG/LZ)_{10.5}$ films coated beads than that from $(ALG/LZ)_5$ or $(ALG/LZ)_{5.5}$ films coated beads, because total amount of LZ assembled on former beads was more than that on latter beads. Consequently, the amount of LZ released from the beads partially depended on the total amount of LZ in the beads when the release time was long enough. Besides, after long time immersion, more LZ could be released via the pores on the beads that suggests the open pore structure could be related the different LZ release behaviors from coated beads [44].

On the contrary, during the short time immersion (Fig. 6a), the amount of released LZ was affected by the amount of LZ assembled on the outermost layer of the beads. Hence, more LZ could be released from $(ALG/LZ)_5$ or $(ALG/LZ)_{5.5}$ films coated beads than that from $(ALG/LZ)_{10}$ or $(ALG/LZ)_{10.5}$ films coating. The reason was as follows: ALG-LZ beads had higher positive charge and larger specific surface area than LBL structured beads, so the thick and large amount of ALG could be assembled on the surface of ALG-LZ beads in the first step of LBL process, which would adsorb

more LZ in the next step. Notably, the LZ assembled on the surface of the beads was less than that in ALG-LZ beads. When the second layer (ALG) was deposited, its amount was less than that of ALG in the former layer. Therefore, the amount of LZ assembled on each bilayer decreased with increasing the number of coating bilayers.

In Fig. 6, especially 24 h later the amount of LZ released from LBL structured beads reduced more or less. The reason was that several free LZ in the solution could be reabsorbed onto the surface of the beads. The result was identical with previous report [45].

4. Conclusion

ALG-LZ beads were selected as the template and modified with negatively charged ALG and positively charged LZ through LBL self-assembly technology. The morphology of LBL films coated ALG-LZ beads was affected by the composition of the outermost layer of the beads. The BET surface area results proved that the ALG and LZ were successfully assembled on the surface of ALG-LZ beads. Surface porosity and phosphate ions had significant influences on the release of LZ. *In vitro* release assay indicated that immobilized LZ could be released into aqueous solutions from both ALG-LZ beads and LBL films coated beads, and the immobilized LZ still maintained its enzymatic activity, which could be used for the nutrition delivery, drug-loading, catalysis, antimicrobial, *etc*.

Acknowledgements

This project was funded by the Open Research Fund Program of Hubei-MOST KLOS & KLOBME.

References

1. H. J. Lee, Y. H. Park and W. G. Koh, *Adv Funct Mater*, 2013, **23**, 652.
2. J. E. Galán and A. Collmer, *Science*, 1999, **284**, 1322.
3. Y. Li, J. Zheng, H. Xiao and D. J. McClements, *Food Hydrocolloids*, 2012, **27**, 517.
4. T. Sessler, J. Weiss and Y. Vodovotz, *Food Hydrocolloids*, 2013.
5. V. R. Sinha and A. Trehan, *Journal of Controlled Release*, 2003, **90**, 261.
6. M. Ye, S. Kim and K. Park, *Journal of Controlled Release*, 2010, **146**, 241.
7. Y. Li and D. J. McClements, *Food Hydrocolloids*, 2013.
8. G. Ma, D. Fang, Y. Liu, X. Zhu and J. Nie, *Carbohydr Polym*, 2012, **87**, 737.
9. L. Salvia-Trujillo, M. A. Rojas-Graü, R. Soliva-Fortuny and O. Martín-Belloso, *Food Hydrocolloids*, 2012.
10. P. de Vos, M. M. Faas, B. Strand and R. Calafiore, *Biomaterials*, 2006, **27**, 5603.
11. S. Sershen and J. West, *Adv Drug Delivery Rev*, 2002, **54**, 1225.
12. S. Singh and J. Singh, *Int J Pharm*, 2004, **271**, 189.
13. K. Zhu, T. Ye, J. Liu, Z. Peng, S. Xu, J. Lei, H. Deng and B. Li, *Int J Pharm*, 2013, **441**, 721.
14. W. Huang, X. Li, Y. Xue, R. Huang, H. Deng and Z. Ma, *Int J Biol Macromol*, 2013, **53**, 26.
15. Y. Li, S. Kadam, T. Abee, T. M. Slaghek, J. W. Timmermans, M. A. Cohen Stuart, W. Norde and M. J. Kleijn, *Food Hydrocolloids*, 2012, **28**, 28.

16. R. Jayakumar, M. Prabaharan, P. Sudheesh Kumar, S. Nair and H. Tamura, *Biotechnol Adv*, 2011, **29**, 322.
17. Q.-Q. Gai, F. Qu, Z.-J. Liu, R.-J. Dai and Y.-K. Zhang, *J Chromatogr A*, 2010, **1217**, 5035.
18. N. Charernsriwilaiwat, P. Opanasopit, T. Rojanarata and T. Ngawhirunpat, *Int J Pharm*, 2012, **427**, 379.
19. W. Huang, H. Xu, Y. Xue, R. Huang, H. Deng and S. Pan, *Food Res Int*, 2012, **48**, 784.
20. H. Deng, X. Zhou, X. Wang, C. Zhang, B. Ding, Q. Zhang and Y. Du, *Carbohydr Polym*, 2010, **80**, 474.
21. W. Li, X. Li, T. Wang, X. Li, S. Pan and H. Deng, *Eur Polym J*, 2012, **48**, 1846.
22. K. Ariga, Y. M. Lvov, K. Kawakami, Q. Ji and J. P. Hill, *Advanced Drug Delivery Reviews*, 2011, **63**, 762.
23. K. Ariga, J. P. Hill and Q. Ji, *Macromolecular bioscience*, 2008, **8**, 981.
24. K. Ariga, J. P. Hill and Q. Ji, *Physical Chemistry Chemical Physics*, 2007, **9**, 2319.
25. R. Huang, Y. Li, X. Zhou, Q. Zhang, H. Jin, J. Zhao, S. Pan and H. Deng, *Carbohydr Polym*, 2012, **90**, 957.
26. X. W. Shi, Y. M. Du, L. P. Sun, J. H. Yang, X. H. Wang and X. L. Su, *Macromolecular bioscience*, 2005, **5**, 881.
27. A. Gupta, C. D. Saquing, M. Afshari, A. E. Tonelli, S. A. Khan and R. Kotek,

Macromolecules, 2009, **42**, 709.

28. C. Pérez, P. De Jesús and K. Griebenow, *Int J Pharm*, 2002, **248**, 193.

29. M. Tachibana, Y. Kobayashi, T. Shimazu, M. Ataka and K. Kojima, *J Cryst Growth*, 1999, **198**, 661.

30. R. Xu, X. Feng, W. Li, S. Xin, X. Wang, H. Deng and L. Xu, *Journal of Biomaterials Science, Polymer Edition*, 2013, **24**, 1.

31. S. Xin, X. Li, Z. Ma, Z. Lei, J. Zhao, S. Pan, X. Zhou and H. Deng, *Carbohydr Polym*, 2013, **92**, 1880.

32. A. Bohr, J. Kristensen, M. Dyas, M. Edirisinghe and E. Stride, *J. R. Soc. Interface*, 2012, **9**, 2437.

33. W. R. Gombotz and S. F. Wee, *Advanced drug delivery reviews*, 2012, **64**, 194.

34. W. Li, X. Li, Y. Chen, X. Li, H. Deng, T. Wang, R. Huang and G. Fan, *Carbohydr Polym*, 2013, **92**, 2232.

35. A. Gole, J. Thakar and M. Sastry, *Colloids and Surfaces B: Biointerfaces*, 2003, **28**, 209.

36. H.-M. Ding, L. Shao, R.-J. Liu, Q.-G. Xiao and J.-F. Chen, *J Colloid Interface Sci*, 2005, **290**, 102.

37. C. Pérez and K. Griebenow, *J Pharm Pharmacol*, 2001, **53**, 1217.

38. L. A. Wells and H. Sheardown, *Eur J Pharm Biopharm*, 2007, **65**, 329.

39. X. Huang and C. S. Brazel, *J Controlled Release*, 2001, **73**, 121.

40. J.-W. Wang and M.-H. Hon, *Journal of Applied Polymer Science*, 2005, **96**,

1083.

41. M. Onda, Y. Lvov, K. Ariga and T. Kunitake, *Biotechnology and bioengineering*, 1996, **51**, 163.

42. W. R. Gombotz and S. Wee, *Adv Drug Delivery Rev*, 1998, **31**, 267.

43. K. Y. Lee and D. J. Mooney, *Progress in polymer science*, 2012, **37**, 106.

44. R. Censi, P. Di Martino, T. Vermonden and W. E. Hennink, *Journal of Controlled Release*, 2012, **161**, 680.

45. R. Xu, S. Xin, X. Zhou, W. Li, F. Cao, X. Feng and H. Deng, *Int J Pharm*, 2012, **438**, 258.

Figure captions:

Scheme 1. Schematic diagram illustrating the fabrication process of LBL films coated ALG-LZ beads.

Fig. 1. The mechanical properties including (A) hardness and (B) resilience of LBL structured beads coated with: $(ALG/LZ)_0$, $(ALG/LZ)_5$, $(ALG/LZ)_{5.5}$, $(ALG/LZ)_{10}$ and $(ALG/LZ)_{10.5}$. Data shown are the mean ± standard deviations (n =3). Significant difference: $^{**}p < 0.01$.

Fig. 2. SEM morphology of LBL structured beads coated with: (a) $(ALG/LZ)_0$, (b) $(ALG/LZ)_{5.5}$, (c) $(ALG/LZ)_{10}$, (d) $(ALG/LZ)_{10.5}$. Images (e) and (f) showed high magnification image and internal section of $(ALG/LZ)_{10.5}$, respectively.

Fig. 3. Nitrogen adsorption and desorption isotherms at 77.3K of: (a) $(ALG/LZ)_0$, (b) $(ALG/LZ)_5$ and (c) $(ALG/LZ)_{10.5}$ film-coated beads, respectively. BJH pore size distribution images derived from the adsorption isotherm were shown: (a') $(ALG/LZ)_0$, (b') $(ALG/LZ)_5$ and (c') $(ALG/LZ)_{10.5}$ film-coated beads, respectively.

Fig. 4. FT-IR Spectra of LBL structured beads coated with: (a) $(ALG/LZ)_0$, (b) $(ALG/LZ)_5$ and (c) $(ALG/LZ)_{10.5}$.

Fig. 5. The enzymatic activity of immobilized LZ of LBL structured beads coated with: $(ALG/LZ)_0$, $(ALG/LZ)_5$, $(ALG/LZ)_{5.5}$, $(ALG/LZ)_{10}$ and $(ALG/LZ)_{10.5}$. Significant difference: $^{**}p < 0.01$.

Fig. 6. Release profiles of LZ from LBL structured beads (a) every 4 h and (b) every 24 h. Data shown are the mean ± standard deviations (n =3).

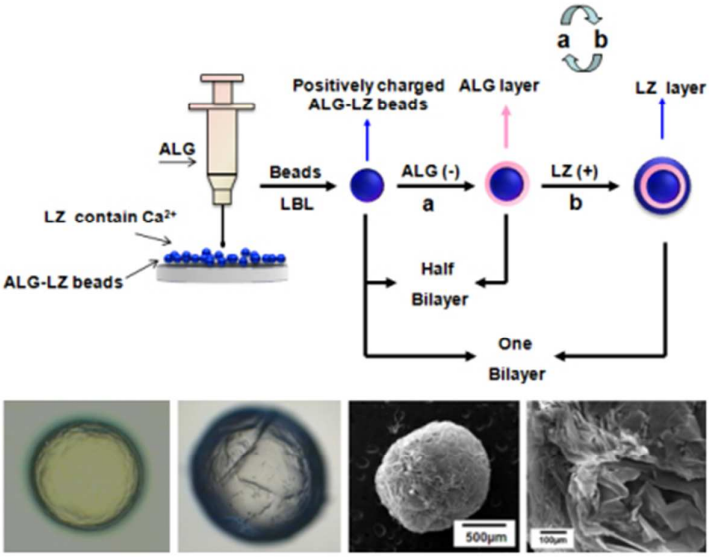

Scheme. 1

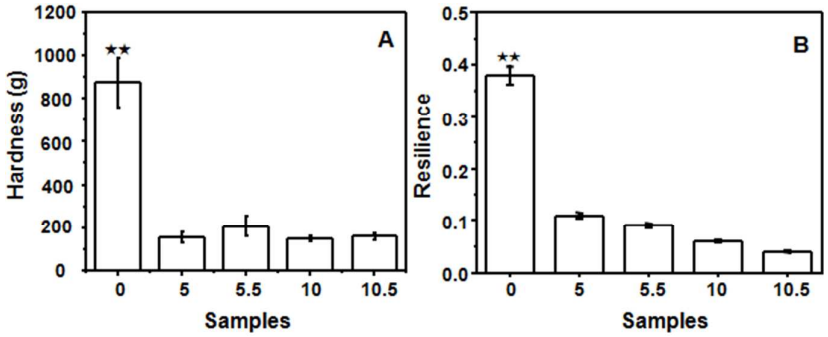

Fig. 1

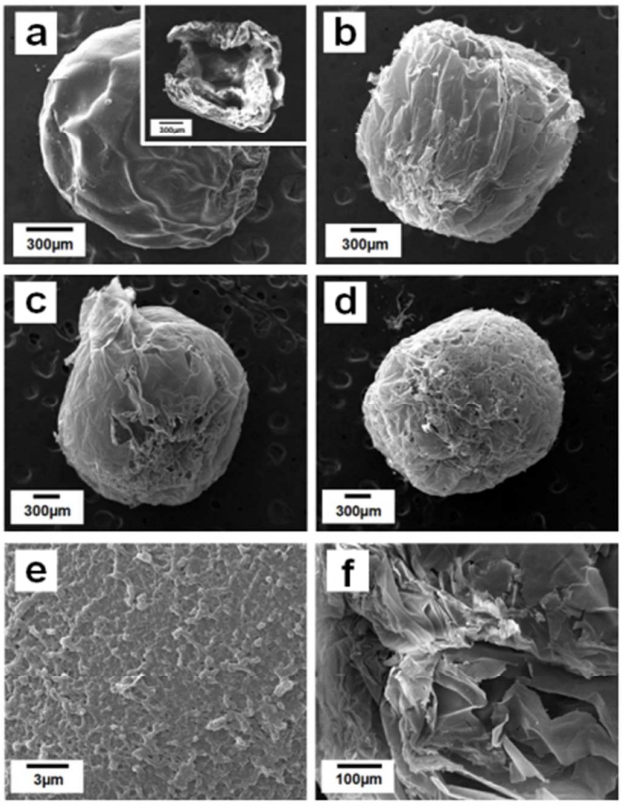

475

476 **Fig. 2**

477

478

479

480

481

482

483

484

485

486

487

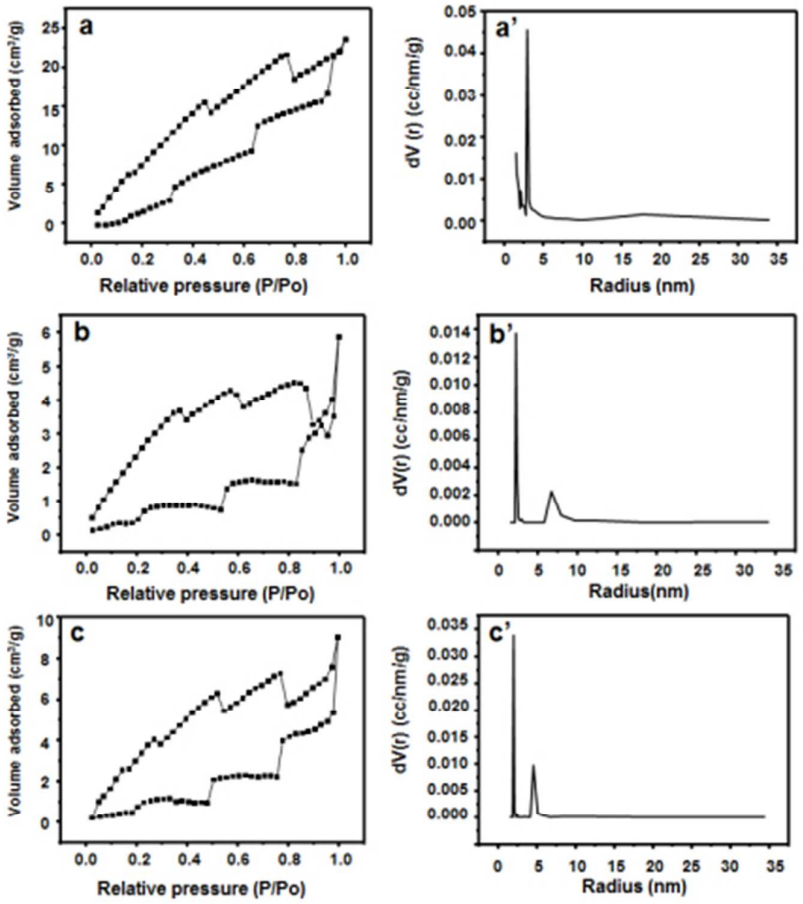

Fig. 3

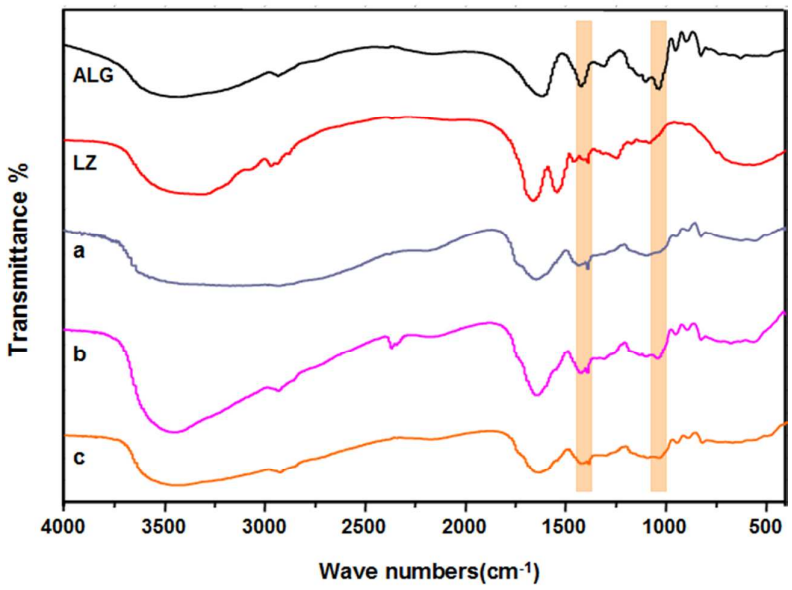

Fig. 4

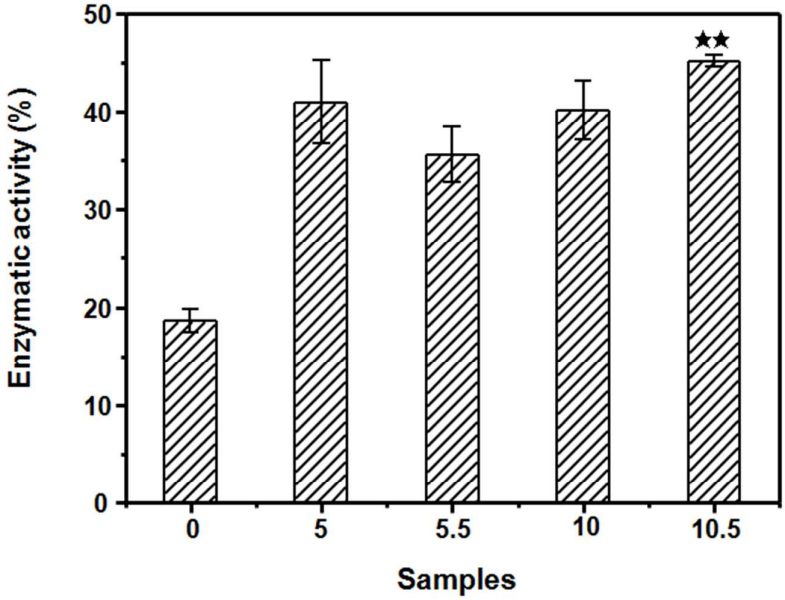

Fig. 5

526

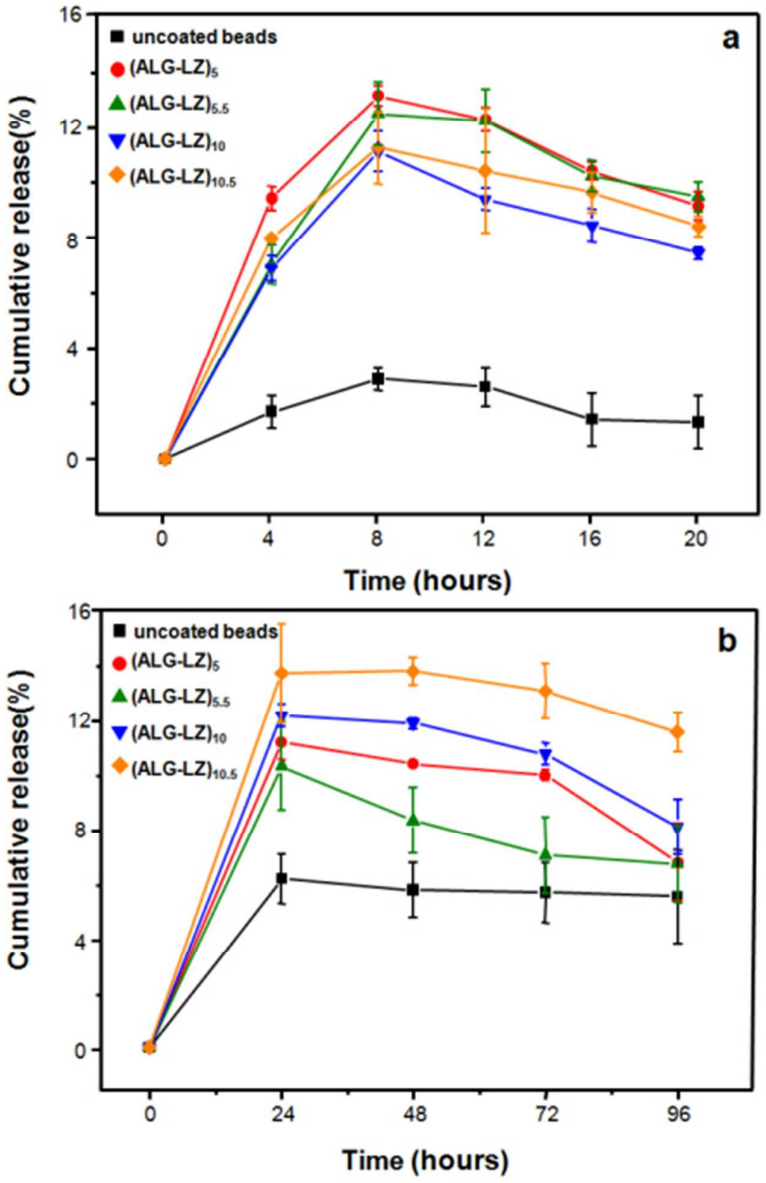

527

528 **Fig. 6**

529

530

531

532

533

534

535 **Tables**

536 **Table 1.** Particle size of beads

Beads coated with LBL films	Average Diameter (mm)	
	Wet beads	Freeze dried beads
$(ALG/LZ)_0$	1.50 ± 0.09	1.25 ± 0.03
$(ALG/LZ)_5$	2.62 ± 0.07	2.34 ± 0.03
$(ALG/LZ)_{5.5}$	2.74 ± 0.03	2.45 ± 0.03
$(ALG/LZ)_{10}$	2.76 ± 0.02	2.52 ± 0.05
$(ALG/LZ)_{10.5}$	2.83 ± 0.12	2.67 ± 0.14

537 Data shown are the mean ± SD (n = 10), measured with a micrometer.

538

539